

# An estimation of the $^{18}\text{O}/^{16}\text{O}$ ratio of UT/LMS ozone based on artefact CO in air sampled during CARIBIC flights

S. Gromov<sup>1</sup>, C. A. M. Brenninkmeijer<sup>1</sup>

<sup>1</sup> Max Planck Institute for Chemistry, Mainz, Germany

Correspondence to: S. Gromov ([sergey.gromov@mpic.de](mailto:sergey.gromov@mpic.de))

## Abstract

An issue of O<sub>3</sub>-driven artefact production of CO in the upper troposphere/lowermost stratosphere (UT/LMS) air analysed in the CARIBIC-1 project is being discussed. By confronting the CO mixing and isotope ratios obtained from different analytical instrumentation, we (i) reject natural/artificial sampling and mixing effects as possible culprits of the problem, (ii) ascertain the chemical nature and quantify the strength of the contamination, and (iii) demonstrate successful application of the isotope mass-balance calculations for inferring the isotope composition of the contamination source. The  $\delta^{18}\text{O}$  values of the latter indicate the oxygen likely being inherited from O<sub>3</sub>. The  $\delta^{13}\text{C}$  values hint at reactions of trace amounts of organics with stratospheric O<sub>3</sub> that could have yielded the artificial CO. While the exact contamination mechanism is not known, it is clear that the issue pertains only to the earlier (first) phase of the CARIBIC project. Finally, estimated UT/LMS ozone  $\delta^{18}\text{O}$  values are lower than those observed in the stratosphere within the same temperature range, suggesting that higher pressures (240–270 hPa) imply lower isotope fractionation controlling the local  $\delta^{18}\text{O}(\text{O}_3)$  value.

## 1 Introduction

[1] Accurate determination of the atmospheric carbon monoxide (CO) mixing ratio based on the collection of air samples depends on the preservation of the mixing ratio of CO inside the receptacle, from the point of sampling to the moment of physicochemical analysis in a laboratory. A well known example in our field of research is the filling of pairs of glass flasks at South Pole

20 Station for analysis at NOAA in Boulder, Colorado, USA (Novelli *et al.*, 1998). There, the du-  
21 plicate air sampling allowed for a degree of quality control which in view of the long transit  
22 times, especially during polar winter, was a perhaps not perfect, but certainly a practical meas-  
23 ure. Here we deal with a different case: Using aircraft-based collection of very large air samples  
24 rendered duplicate sampling unpractical, yet analyses could be performed soon after the sam-  
25 pling had taken place because of the proximity of the aircraft's landing location to the laborato-  
26 ry involved. A presumption of the analytical integrity of the process was that the growth of CO  
27 in receptacles is gradual and takes its time. Reminding Thomas Henry Huxley's statement, "The  
28 great tragedy of Science – the slaying of a beautiful hypothesis by an ugly fact", it turned out,  
29 however, that for air we collected in stainless steel tanks in the upper troposphere/lowermost  
30 stratosphere (UT/LMS) higher CO values were measured in the laboratory than measured  
31 *in situ* during the collection of these air samples. Moreover, measurement of the stable oxygen  
32 isotopic composition of CO from these tanks revealed additional isotopic enrichments in  $^{18}\text{O}$  of  
33 10‰ or more. It was soon realised that this phenomenon was due to the formation of CO in  
34 these tanks and/or possibly in the sampling system and inlet tubing used, by reactions involving  
35 ozone (Brenninkmeijer *et al.*, 1999).

36 [2] Unexpectedly high  $^{18}\text{O}/^{16}\text{O}$  ratios in stratospheric ozone ( $\text{O}_3$ ) were discovered by Konrad  
37 Mauersberger using a balloon-borne mass spectrometer (Mauersberger, 1981), which has trig-  
38 gered a series of theoretical and experimental studies on atmospheric  $\text{O}_3$  heavy isotope enrich-  
39 ments (see, *e.g.*, Schinke *et al.* (2006) for a review). In view of the advances in theoretical and  
40 laboratory studies on the isotopic composition of  $\text{O}_3$  atmospheric measurements are welcome,  
41 they do however form a challenge. In the stratosphere  $\text{O}_3$  number concentrations are high, but  
42 the remoteness of the sampling domain is a problem. In the troposphere, low  $\text{O}_3$  number densi-  
43 ties are the main obstacle, as indicated by few experiments performed to date  
44 (Krankowsky *et al.*, 1995; Johnston and Thiemens, 1997; Vicars and Savarino, 2014). Never-  
45 theless, recent analytical improvements, namely the use of an indirect method of reacting at-  
46 mospheric  $\text{O}_3$  with a substrate that can be analysed for the isotopic composition of the  
47  $\text{O}_3$ -derived oxygen (Vicars *et al.*, 2012), has greatly improved our ability to obtain information  
48 on the  $\text{O}_3$  isotopic composition.

49 [3] Although the increase of CO concentrations in air stored in vessels is a well recognised  
50 problem, to our knowledge a specific  $\text{O}_3$ -related process has not been reported yet. Here we dis-  
51 cuss this phenomenon and turn its disadvantage into an advantage, namely that of obtaining an  
52 estimate of the oxygen isotopic composition of  $\text{O}_3$  in the UT/LMS, an atmospheric domain not

53 yet covered by specific measurements. The air samples we examine in this study were collected  
54 onboard a passenger aircraft carrying an airfreight container with analytical and air/aerosol  
55 sampling equipment on long distance flights from Germany to South India and the Caribbean  
56 within the framework of the CARIBIC project (Civil Aircraft for the Regular Investigation of  
57 the atmosphere Based on an Instrument Container, <http://www.caribic-atmospheric.com>).

## 58 **2 Experimental and results**

### 2.1 Whole air sampling

59 [4] CARIBIC-1 (Phase #1, abbreviated hereafter “C1”) was operational from November 1998  
60 until April 2002 using a *Boeing 767-300 ER* operated by LTU International Airlines  
61 (Brenninkmeijer *et al.*, 1999). Using a whole air sample (WAS) collection system, twelve air  
62 samples were collected per flight (of 8–10 hours duration at cruise altitudes of 10–12 km) in  
63 stainless steel tanks for subsequent laboratory analysis of the mixing ratios (*i.e.* mole fractions)  
64 of various trace gases, including  $^{14}\text{CO}$ . Large air samples were required in view of the ultra-low  
65 number density of this mainly cosmogenic tracer (10–100 molecules  $\text{cm}^{-3}$  standard temperature  
66 and pressure (STP), about 0.4–4 amol/mol). Hereinafter STP denotes dry air at 273.15 K,  
67 101325 Pa. Each C1 WAS sample (holding 350 litres of air STP) was collected over 15–20 min  
68 intervals representing the number density-weighted average of the compositions encountered  
69 along flight segments of about 250 km. The overall uncertainty of the measured WAS CO is  
70 less than  $\pm 1\%$  for the mixing ratio and  $\pm 0.1\text{‰}/\pm 0.2\text{‰}$  for  $\delta^{13}\text{C}(\text{CO})/\delta^{18}\text{O}(\text{CO})$ , respectively  
71 (Brenninkmeijer, 1993; Brenninkmeijer *et al.*, 2001). Isotope compositions are reported  
72 throughout this manuscript using the so-called delta value  $\delta = (R/R_{\text{st}} - 1)$  relating the ratio  $R$  of  
73 rare ( $^{13}\text{C}$ ,  $^{18}\text{O}$  or  $^{17}\text{O}$ ) over abundant isotopes of interest to the standard ratio  $R_{\text{st}}$ . These are Vi-  
74 enna Standard Mean Ocean Water for  $^{18}\text{O}/^{16}\text{O}$  (Gonfiantini, 1978; Coplen, 1994) and  $^{17}\text{O}/^{16}\text{O}$   
75 (Assonov and Brenninkmeijer, 2003), and Vienna Pee Dee Belemnite for  $^{13}\text{C}/^{12}\text{C}$  (Craig, 1957),  
76 respectively. As we mention above, the oxygen isotope composition of the CO present in these  
77 WAS samples was corrupted, in particular when  $\text{O}_3$  levels were as high as 100–600 nmol/mol.

78 [5] CARIBIC-2 (Phase #2, referred to as “C2”) started operation in December 2004 with a  
79 Lufthansa *Airbus A340-600* fitted with a new inlet system and air sampling lines, including per-  
80 fluoroalkoxy alkane (PFA) lined tubing for trace gas intake (Brenninkmeijer *et al.*, 2007). No  
81 flask CO mixing/isotope ratio measurements are performed in C2.

## 2.2 On-line instrumentation

82 [6] In addition to the WAS collection systems, both C1 and C2 measurement setups include dif-  
83 ferent instrumentation for on-line detection of [CO] and [O<sub>3</sub>] (hereinafter the squared brackets  
84 [] denote the mixing ratio of the respective species). *In situ* CO analysis in C1 is done using a  
85 gas chromatography (GC)-reducing gas analyser which provides measurements every 130 s  
86 with an uncertainty of  $\pm 3$  nmol/mol (Zahn *et al.*, 2000). In C2, a vacuum ultraviolet fluores-  
87 cence (VUV) instrument with lower measurement uncertainty and higher temporal resolution of  
88  $\pm 2$  nmol/mol in 2 s (Scharffe *et al.*, 2012) is employed. Furthermore, the detection frequency  
89 for O<sub>3</sub> mixing ratios has also increased, *viz.*, from 0.06 Hz in C1 to 5 Hz in C2  
90 (Zahn *et al.*, 2002; Zahn *et al.*, 2012).

## 2.3 Results

91 [7] When comparing the CO mixing ratios in relation to those of O<sub>3</sub> for C1 and C2, differences  
92 are apparent in the LMS, where C2 [CO] values are systematically lower. This is illustrated in  
93 Fig. 1 (a) which presents the LMS CO-O<sub>3</sub> distribution of the C2 *in situ* measurements overlaid  
94 with the C1 *in situ* and WAS data. The entire C1 CO/O<sub>3</sub> dataset is presented in Fig. 2. For the  
95 *in situ* CO datasets we calculated the statistics (Fig. 1 (b)) of the samples with respective O<sub>3</sub>  
96 mixing ratios clustered in 20 nmol/mol bins, *i.e.* the median and spread of [CO] as a function of  
97 [O<sub>3</sub>] analysed. The interquartile range, IQR, is used in the current analysis as a robust measure  
98 of the data spread instead of the standard deviation. The data exhibit large [CO] variations at  
99 [O<sub>3</sub>] below 400 nmol/mol that primarily reflect pronounced seasonal variations in the NH tropo-  
100 spheric CO mixing ratio. With increasing [O<sub>3</sub>], [CO] decreases to typical stratospheric values,  
101 and its spread reduces to mere 3.5 nmol/mol and less, as [O<sub>3</sub>] surpasses 500 nmol/mol. Despite  
102 the comparable spread in C1 and C2 [CO], from 400 nmol/mol of [O<sub>3</sub>] onwards the C1 CO mix-  
103 ing ratios start to level off, with no samples below 35 nmol/mol having been detected, whereas  
104 the C2 levels continuously decline. By the 580 nmol/mol O<sub>3</sub> bin, C1 [CO] of  $39.7^{+9.3}$  nmol/mol  
105 contains some extra 15 nmol/mol compared to  $25.6^{+1.7}$  nmol/mol typical for C2 values. Overall,  
106 at [O<sub>3</sub>] above 400 nmol/mol the conspicuously high [CO] is marked in about 200 *in situ* C1  
107 samples, of which 158 and 69 emerge as statistically significant mild and extreme outliers, re-  
108 spectively, when compared against the number of C2 samples ( $n > 3 \cdot 10^5$ ). The conventions here  
109 follow Natrella (2003), *i.e.*  $\pm 1.5$  and  $\pm 3$  IQR ranges define the inner and outer statistical fences  
110 (ranges outside which the data points are considered mild and extreme outliers) of the C2 [CO]  
111 distribution in every O<sub>3</sub> bin, respectively. The statistics include the samples in bins with average

112 [O<sub>3</sub>] of 420–620 nmol/mol. None of C1 CO at [O<sub>3</sub>] above 560 nmol/mol agrees with the C2 ob-  
113 servations. Because the CO-O<sub>3</sub> distribution cannot have changed over the period in question, we  
114 find that an apparent relative excess CO of up to 55% justifies and investigation into sampling  
115 artefacts and calibration issues.

116 [8] Unnatural elevations in  $\delta^{18}\text{O}(\text{CO})$  from WAS measurements are also evident, as shown in  
117 Figs. 3 and 4. The large  $\delta^{18}\text{O}(\text{CO})$  elevations that reach beyond +16‰ are found to be propor-  
118 tional to the concomitant O<sub>3</sub> mixing ratios (denoted with colour) and are more prominent at  
119 lower [CO]. Lower  $\delta^{18}\text{O}(\text{CO})$  values, however, are expected based on our knowledge of UT/  
120 LMS CO sources (plus their isotope signatures) and available *in situ* observations (Fig. 3,  
121 shown with triangles), as elucidated by Brenninkmeijer *et al.* (1996) (hereafter denoted as  
122 “B96”). That is, the greater the proportion of stratospheric CO, the greater its fraction stemming  
123 from methane oxidation with a characteristic  $\delta^{18}\text{O}$  of 0‰ or lower (Brenninkmeijer and Röck-  
124 mann, 1997). This occurs because the CO sink at ruling UT/LMS temperatures proceeds more  
125 readily than its production, as the reaction of hydroxyl radical (OH) with CO, being primarily  
126 pressure-dependent, is faster than the temperature-sensitive reaction of OH with CH<sub>4</sub>. Further-  
127 more, as the lifetime of CO quickly decreases with altitude, transport-mixing effects take the  
128 lead in determining the vertical distributions of [CO] and  $\delta^{18}\text{O}(\text{CO})$  above the tropopause,  
129 hence their mutual relationship. This is seen from the B96 data at [CO] below 50 nmol/mol that  
130 line-up in a near linear relationship towards the end-members with lowest <sup>18</sup>O/<sup>16</sup>O ratios. These  
131 result from the largest share of the <sup>18</sup>O-depleted photochemical component and extra depletion  
132 caused by the preferential removal of C<sup>18</sup>O in reaction with OH (fractionation about +11‰ at  
133 pressures below 300 hPa, Stevens *et al.*, 1980; Röckmann *et al.*, 1998b).

134 [9] We are confident that the enhancements of C1 C<sup>18</sup>O originate from O<sub>3</sub>, whose large enrich-  
135 ment in <sup>18</sup>O (above +60‰ in  $\delta^{18}\text{O}$ , Brenninkmeijer *et al.*, 2003) is typical and found transferred  
136 to other atmospheric compounds (see Savarino and Morin (2012) for a review). In Fig. 3 it is al-  
137 so notable that not only the LMS compositions are affected but elevations of (3–10)‰ from the  
138 bulk  $\delta^{18}\text{O}(\text{CO})$  values are present in more tropospheric samples with [CO] of up to  
139 100 nmol/mol. These result from the dilution of the least affected CO-rich tropospheric air by  
140 CO-poor, however substantially contaminated, stratospheric air, sampled into the same WAS  
141 tank. Such sampling-induced mixing renders an unambiguous determination of the artefact  
142 source’ isotope signature rather difficult, because neither mixing nor isotope ratios of the ad-  
143 mixed air portions are known sufficiently well (see below).

144 [10] Differences between the WAS and *in situ* measured [CO] – a possible indication that the  
145  $\delta^{18}\text{O}(\text{CO})$  contamination pertains specifically to the WAS data – average at  $\bar{\Delta}(\text{WAS}-\textit{in situ}) =$   
146  $(5.3 \pm 0.2)$  nmol/mol ( $\pm 1$  standard deviation of the mean,  $n = 408$ ) and happen to be random with  
147 respect to any operational parameter or measured characteristic in C1, *i.e.* irrespective of CO or  
148  $\text{O}_3$  abundances. The above mentioned discrepancy remained after several calibrations between  
149 the two systems had been performed, and likely results from the differences in the detection  
150 methods, drifts of the calibration standards used (see details in Brenninkmeijer *et al.*, 2001) and  
151 a short-term production of CO in the stainless steel tanks during sampling. The large spread of  
152  $\Delta(\text{WAS}-\textit{in situ})$  of  $\pm 3.5$  nmol/mol ( $\pm 1\sigma$  of the population) ensues from the fact that the *in situ*  
153 sampled air corresponds to (2–4)% of the concomitantly sampled WAS volume, as typically  
154 6–7 *in situ* collections of 5 s were made throughout one tank collection of 17–21 min. The in-  
155 tegrity of the WAS CO is further affirmed by the unsystematic distribution of the artefact com-  
156 positions among tanks (in contrast to that for  $\delta^{18}\text{O}(\text{CO}_2)$  in C1 discussed by As-  
157 sonov *et al.*, 2009). Overall, the WAS and *in situ* measured CO mixing ratios correlate extreme-  
158 ly well (adj.  $R^2 = 0.972$ , slope of  $0.992 \pm 0.008$  ( $\pm 1\sigma$ ),  $n = 408$ ). However, both anomalies in  
159 [CO] and  $\delta^{18}\text{O}(\text{CO})$  manifest clear but complex influences of the concomitant [ $\text{O}_3$ ]. That is, the  
160 C1 *in situ* and WAS data very likely evidence artefacts pertaining to the  $\text{O}_3$ -driven effect of the  
161 same nature. Below we discuss and quantify these influences.

### 162 3 Discussion

163 [11] Three factors may lead to the (artefact) distributions seen for C1 *in situ* [CO] at LMS  $\text{O}_3$   
164 mixing ratios, namely:

165 [12] (i) Strong (linear) natural mixing, such as enhanced stratosphere-troposphere exchange  
166 (STE), when a [CO] outside the statistically expected range results from the integration of air  
167 having dissimilar ratios of the tracers' mixing ratios, *viz.* [ $\text{O}_3$ ]:[CO]. For example, mixing of  
168 two air parcels in a 16%:84% proportion (by moles of air) with typical [ $\text{O}_3$ ]:[CO] of 700:24  
169 (stratospheric) and 60:125 (tropospheric), respectively, yields an integrated composition with  
170 [ $\text{O}_3$ ]:[CO] of 598:40 which indeed corresponds to C1 data (this case is exemplified by the mix-  
171 ing curve in Fig. 1). Nonetheless, occurrences of rather high stratospheric CO mixing ratios (in  
172 our case, 40 nmol/mol at the concomitant [ $\text{O}_3$ ] of 500–600 nmol/mol compared to the typical  
173 24–26 nmol/mol) are rare. For instance, a deep STE similar to that described by  
174 Pan *et al.* (2004) was observed by C2 only once (*cf.* the outliers at [ $\text{O}_3$ ] of 500 nmol/mol in  
175 Fig. 1), whereas the C1 outliers were exclusively registered in some 12 flights during

176 1997–2001. No relation between these outliers and the large-scale [CO] perturbation due to ex-  
177 tensive biomass burning in 1997/1998 (Novelli *et al.*, 2003) is established, otherwise elevated  
178 CO mixing ratios should manifest themselves at lower [O<sub>3</sub>] as well. Other tracers detected in  
179 CARIBIC provide supporting evidence against such strongly STE-mixed air having been cap-  
180 tured by C1. That is, the binned distributions for water vapour and de-trended N<sub>2</sub>O mixing rati-  
181 os (not shown here) are similar for C1 and C2. Whereas the small relative variations in atmos-  
182 pheric [N<sub>2</sub>O] merely confirm matching [O<sub>3</sub>] distributions in CARIBIC, the stratospheric [H<sub>2</sub>O]  
183 distributions witness no [O<sub>3</sub>]:[H<sub>2</sub>O] values corresponding to those of the C1 outliers, suggesting  
184 the latter being unnaturally low.

185 [13] (ii) Mixing effects can also occur artificially, originating from sampling peculiarities or data  
186 processing. Since the CARIBIC platform is not stationary, about 5 s long sampling of an *in situ*  
187 air probe in C1 implies integration of the air compositions encountered along some hundred me-  
188 tres, owing to the high aircraft speed. This distance may cover a transect between tropospheric  
189 and stratospheric filaments of different compositions. The effect of such ‘translational mixing’  
190 can be simulated by averaging the sampling data with higher temporal frequency over longer  
191 time intervals. In this respect, the substantially more frequent CO data in C2 (sampling interval  
192 <1 s) were artificially averaged over a set of increasing intervals to reckon whether the long  
193 sampling period in C1 could be the culprit for skewing its CO–O<sub>3</sub> distribution. As a result, the  
194 original C2 data and their averages (equivalent to the C1 CO sample injection time) differ neg-  
195 ligibly, as do the respective [O<sub>3</sub>]:[CO] values. Our simulations of the ‘translational mixing’ ef-  
196 fects confirm that the actual C2 CO–O<sub>3</sub> distribution in the region of interest ([O<sub>3</sub>] of  
197 540–620 nmol/mol) remains insensitive to averaging intervals of up to 300 s. Furthermore, a  
198 very strong artificial mixing with an averaging interval of at least 1200 s (comparable to C1  
199 WAS sampling time) is required to yield the averages from the C2 data with [O<sub>3</sub>]:[CO] charac-  
200 teristic for the C1 outliers.

201 [14] (iii) In view of the above, it is unlikely that any natural or artificial mixing processes are in-  
202 volved in the stratospheric [CO] discrepancies seen in C1. We therefore conclude that the sam-  
203 ple contamination in C1 occurred prior to the probed air reaching the analytical instrumentation  
204 and WAS sampling tanks in the container, since clearly elevated stratospheric CO mixing ratios  
205 are common to WAS and *in situ* data. Two more indications, *viz.* growing [CO] discrepancy  
206 with increasing O<sub>3</sub> abundance, and the strong concomitant signal in δ<sup>18</sup>O(CO), suggest that O<sub>3</sub>-  
207 mediated production of CO took place. Further, by confronting the C1 and C2 [CO] measure-

208 ments in a regression analysis (detailed in Appendix A), we quantify the artefact component  
 209  $[\text{CO}]_c$  being chiefly a function of  $\text{O}_3$  mixing ratio as

$$[\text{CO}]_c = b \cdot [\text{O}_3]^2, \quad b = (5.19 \pm 0.12) \cdot 10^{-5} \text{ [mol/nmol]}, \quad (1)$$

210 which is equivalent to 8–18 nmol/mol throughout the respective  $[\text{O}_3]$  range of  
 211 400–620 nmol/mol (see Fig. 1 (d)). Subtracting this artefact signal yields the corrected *in situ*  
 212 C1 CO– $\text{O}_3$  distribution conforming to that of C2 (*cf.* red symbols in Fig. 1 (a)).

213 [15] Importantly, since we can quantify the contamination strength using only the  $\text{O}_3$  mixing ra-  
 214 tio, the continuous *in situ* C1  $[\text{O}_3]$  data allow estimating the integral artefact CO component in  
 215 each WAS sample and, if the isotope ratio of contaminating  $\text{O}_3$  is known, to derive the initial  
 216  $\delta^{18}\text{O}(\text{CO})$ . The latter, as it was mentioned above, is subject to strong sample-mixing effects,  
 217 which is witnessed by  $\delta^{18}\text{O}(\text{CO})$  outliers even at relatively high  $[\text{CO}]$  up to 100 nmol/mol. Ac-  
 218 counting for such cases is, however, problematic since it is necessary to distinguish the propor-  
 219 tions of the least modified (tropospheric) and significantly affected (stratospheric) components  
 220 in the resultant WAS sample mix. Since this information is not available, we applied an *ad hoc*  
 221 correction approach, as described in the following. This approach is capable of determining the  
 222 contamination source (*i.e.*,  $\text{O}_3$ ) isotope signature as well.

### 3.1 Contamination isotope signatures

223 [16] We use the differential mixing model (MM, originally known as the “Keeling-plot”), be-  
 224 cause it requires only the estimate of the artefact component mixing ratio, but no assumptions  
 225 on the (unknown) shares and isotope signatures of the air portions mixed in a given WAS tank.  
 226 The MM parameterises the admixing of the portion of artefact CO to the WAS sample with the  
 227 “true” initial composition, as formulated below:

$$[\text{CO}]_a = [\text{CO}]_t + [\text{CO}]_c, \quad (2)$$

$${}^i\delta_a [\text{CO}]_a = {}^i\delta_t [\text{CO}]_t + {}^i\delta_c [\text{CO}]_c, \quad (3)$$

228 where indices  $a$ ,  $c$  and  $t$  distinguish the mixing ratios and isotope compositions  ${}^i\delta$  ( ${}^{18}\delta$  and  ${}^{13}\delta$   
 229 for  ${}^{13}\text{C}$  and  ${}^{18}\text{O}$ , respectively) pertaining to the analysed sample, estimated contamination and  
 230 “true” composition sought (*i.e.*,  $[\text{CO}]_t$  and  ${}^i\delta_t$ ), respectively. Here the contamination strength  
 231  $[\text{CO}]_c$  is derived by integrating Eq. (1) using the *in situ* C1  $[\text{O}_3]$  data for each WAS sample. By  
 232 rewriting the above equation with respect to the isotope signature of the analysed CO, one ob-  
 233 tains:

$${}^i\delta_a = {}^i\delta_c + ({}^i\delta_t - {}^i\delta_c) [\text{CO}]_c / [\text{CO}]_a, \quad (4)$$



234 which signifies that linear regression of  ${}^i\delta_a$  as a function of the reciprocal of  $[\text{CO}]_a$  yields the es-  
235 timated contamination signature  ${}^i\delta_c$  at  $([\text{CO}]_a)^{-1} \rightarrow 0$  when invariable "true" compositions  
236  $([\text{CO}]_t, {}^i\delta_t)$  are taken (the Keeling plot detailing these calculations is shown in Fig. 5). We there-  
237 fore apply the MM described by Eq. (2) to the subsets of samples picked according to the same  
238 reckoned  $[\text{CO}]_t$  (within a  $\pm 2$  nmol/mol window,  $n > 7$ ). Such selection, however, may be insuf-  
239 ficient: Due to the strong sampling effects in the WAS samples (see previous Section), it is pos-  
240 sible to encounter samples that integrate different air masses to the same  $[\text{CO}]_t$  but rather differ-  
241 ent average  ${}^i\delta_t$ . The solution in this case is to refer to the goodness of the MM regression fit, be-  
242 cause the  $R^2$  intrinsically measures the linearity of the regressed data, *i.e.* closeness of the "true"  
243 values in a regarded subset of samples, irrespective of underlying reasons for that.

244 [17] Higher  $R^2$  values thus imply higher consistency of the estimate, as demonstrated in Fig. 6  
245 showing the calculated  ${}^i\delta_c$  for  $[\text{CO}]_t$  below 80 nmol/mol as a function of the regression  $R^2$ . The  
246 latter decreases with greater  $[\text{CO}]_t$  (*i.e.*, larger sample subset size, since tropospheric air is more  
247 often encountered) and, correspondingly, larger variations in  ${}^i\delta_t$ . Ultimately, at lower  $R^2$  the in-  
248 ferred  ${}^{18}\delta_c$  converge to values slightly above zero expected for uncorrelated data, *i.e.* C1  
249  $\delta^{18}\text{O}(\text{CO})$  tropospheric average. A similar relationship is seen for the  ${}^{13}\delta_c$  values (they converge  
250 around  $-28\text{‰}$ ), however, there are no consistent estimates found ( $R^2$  is generally below 0.4).  
251 Since such is not the case for  $\delta^{18}\text{O}$ , the MM is not sufficiently sensitive to the changes caused  
252 by the contamination, which implies that the artefact CO  $\delta^{13}\text{C}$  should be within the range of the  
253 "true"  $\delta^{13}\text{C}(\text{CO})$  values. Interestingly, the MM is rather responsive to the growing fraction of  
254 the  $\text{CH}_4$ -derived component in CO with increasing  $[\text{O}_3]$ , as the  ${}^{13}\delta_c$  value of  $-(47.2 \pm 5.8)\text{‰}$  in-  
255 ferred at  $R^2$  above 0.4 is characteristic for the  $\delta^{13}\text{C}$  of methane in the UT/LMS. It is important to  
256 note that we have accounted for the biases in the analysed C1 WAS  $\delta^{13}\text{C}(\text{CO})$  expected from  
257 the mass-independent isotope composition of  $\text{O}_3$  (see details in Appendix B).

258 [18] We derive the "best-guess" estimate of the admixed CO  ${}^{18}\text{O}$  signature at  ${}^{18}\delta_c =$   
259  $+(92.0 \pm 8.3)\text{‰}$ , which agrees with the other MM results obtained at  $R^2$  above 0.75. Taking the  
260 same subsets of samples, the concomitant  ${}^{13}\text{C}$  signature matches  ${}^{13}\delta_c = -(23.3 \pm 8.6)\text{‰}$ , indeed at  
261 the upper end of the expected LMS  $\delta^{13}\text{C}(\text{CO})$  variations of  $-(25-31)\text{‰}$ . Because of that, the  
262 MM is likely insensitive to the changes in  $\delta^{13}\text{C}(\text{CO})$  caused by the contamination (the corre-  
263 sponding  $R^2$  values are below 0.1). Upon the correction using the inferred  ${}^{18}\delta_c$  value, the C1  
264 WAS  $\delta^{18}\text{O}(\text{CO})$  data agree with B96 (shown with red symbols in Fig. 3). That is, variations in  
265 the observed  $\text{C}^{18}\text{O}$  are driven by (i) the seasonal/regional changes in the composition of tropo-  
266 spheric air and by (ii) the degree of mixing or replacement of the latter with the stratospheric

267 component that is less variable in  $^{18}\text{O}$ . This is seen as stretching of the scattered tropospheric  
268 values ( $[\text{CO}]$  above 60 nmol/mol) towards  $\delta^{18}\text{O}(\text{CO})$  of around  $-10\%$  at  $[\text{CO}]$  of 25 nmol/mol,  
269 respectively. The corrected C1  $\delta^{13}\text{C}(\text{CO})$  data (shown in Fig. 7) are found to be in a  $\pm 1\%$   
270 agreement with the observations by B96, except for several deep stratospheric samples ( $[\text{CO}]$   
271 below 40 nmol/mol). The latter were encountered during “ozone hole” conditions and carried  
272 extremely low  $\delta^{13}\text{C}(\text{CO})$  values, which was attributed to the reaction of methane with available  
273 free Cl radicals (Brenninkmeijer *et al.*, 1996).

### 3.2 Estimate of $\delta^{18}\text{O}(\text{O}_3)$

274 [19] The contamination  $^{18}\text{O}$  signature inferred here ( $^{18}\delta_c = +(92.0 \pm 8.3)\%$ ) likely pertains to  $\text{O}_3$   
275 and is comparable to  $\delta^{18}\text{O}(\text{O}_3)$  values measured in the stratosphere at temperatures about 30 K  
276 lower than those encountered in the UT/LMS by C1 (see Table 1 for comparison). If no other  
277 factors are involved (see below), this discrepancy in  $\delta^{18}\text{O}(\text{O}_3)$  should be attributed to the local  
278 conditions, *i.e.* the higher pressures (typically 240–270 hPa for C1 cruising altitudes) at which  
279  $\text{O}_3$  was formed. Indeed, the molecular lifetime (the period through which the species’ isotope  
280 reservoir becomes entirely renewed, as opposed to the “bulk” lifetime) of  $\text{O}_3$  encountered along  
281 the C1 flight routes is estimated on the order of minutes to hours at daylight (H. Riede, Max  
282 Planck Institute for Chemistry, 2010), thus the isotope composition of the photochemically re-  
283 generated  $\text{O}_3$  resets quickly according to the local conditions. Virtual absence of sinks, in turn,  
284 leads to “freezing” of the  $\delta^{18}\text{O}(\text{O}_3)$  value during night in the UT/LMS. Verifying the current  
285  $\delta^{18}\text{O}(\text{O}_3)$  estimate against the kinetic data, in contrast to the stratospheric cases, is problematic.  
286 The laboratory studies on  $\text{O}_3$  formation to date have scrutinised the concomitant kinetic isotope  
287 effects (KIEs) as a function of temperature at only low pressures (67 mbar); the attenuation of  
288 the KIEs with increasing pressure was studied only at room temperatures (see Table 1, also  
289 Brenninkmeijer *et al.* (2003) for references). A rather crude attempt may be undertaken by as-  
290 suming that the formation KIEs become attenuated at higher pressures in a similar (proportion-  
291 al) fashion to that measured at 320 K, however applied to the nominal low-pressure values  
292 reckoned at (220–230) K. A decrease in  $\delta^{18}\text{O}(\text{O}_3)$  of about (6–8)% is expected from such cal-  
293 culation (*cf.* last row in Table 1), yet accounting for a mere one-half of the (13–15)% discrep-  
294 ancy between the stratospheric  $\delta^{18}\text{O}(\text{O}_3)$  values and  $^{18}\delta_c$ .

295 [20] Lower  $^{18}\delta_c$  values could result from possible isotope fractionation accompanying the pro-  
296 duction of the artefact CO. Although not quantifiable here, oxygen KIEs in the  $\text{O}_3 \rightarrow \text{CO}$  con-  
297 version chain cannot be ruled out, recalling that the intermediate reaction steps are not identifi-

298 able and the artefact CO represents at most 4% of all O<sub>3</sub> molecules. Furthermore, the yield  $\lambda_{\text{O}_3}$   
299 of CO from O<sub>3</sub> may be lower than unity (see details in Appendix A). On the other hand, the in-  
300 ference that the contamination strength primarily depends on [O<sub>3</sub>] indicates that the kinetic frac-  
301 tionation may have greater effect on the carbon isotope ratios of the artefact CO produced (the  
302  $^{13}\delta_c$  values) in contrast to the oxygen ones. That is because all reactive oxygen available from  
303 O<sub>3</sub> becomes converted to CO, whilst the concomitant carbon atoms are drawn from a virtually  
304 unlimited pool whose apparent isotope composition is altered by the magnitude of the  $^{13}\text{C}$  KIEs.

305 [21] Besides KIEs, selectivity in the transfer of O atoms from O<sub>3</sub> to CO affects the resulting  $^{18}\delta_c$   
306 value. The terminal O atoms in O<sub>3</sub> are enriched with respect to the molecular (bulk) O<sub>3</sub> compo-  
307 sition when the latter is above +70‰ in  $\delta^{18}\text{O}$  (Janssen, 2005; Bhattacharya *et al.*, 2008), there-  
308 fore an incorporation of only central O atoms into the artefact CO molecules should result in a  
309 reduced apparent  $^{18}\delta_c$  value. Such exclusive selection is, however, less likely from the kinetic  
310 standpoint and was not observed in available laboratory studies (see Savarino *et al.* (2008) for a  
311 review). For instance, Röckmann *et al.* (1998a) established the evidence of direct O transfer  
312 from O<sub>3</sub> to the CO produced in alkene ozonolysis. A reanalysis of their results (in light of find-  
313 ings of Bhattacharya *et al.* (2008)) suggests that usually the terminal atoms of the O<sub>3</sub> molecule  
314 become transferred (their ratio over the central ones changes from the bulk 2:1 to 1:0 for vari-  
315 ous species). Considering the alternatives of the O transfer in our case (listed additionally in  
316 Table 1), the equiprobable incorporation of the terminal and central O<sub>3</sub> atoms into CO should  
317 result in the  $\delta^{18}\text{O}(\text{O}_3)$  value in agreement with the “crude” estimate based on laboratory data  
318 given above.

319 [22] Furthermore, the conditions that supported the reaction of O<sub>3</sub> (or its derivatives) followed by  
320 the production of CO are vague. A few hypotheses ought to be scrutinised here. First, a fast  
321 O<sub>3</sub> → CO conversion must have occurred, owing to short (*i.e.*, fraction of a second) exposure  
322 time of the probed air to the contamination. Accounting for the typical C1 air sampling condi-  
323 tions (these are: sampled air pressure of 240–270 hPa and temperature of 220–235 K outboard  
324 to 275–300 K inboard, sampling rate of  $12.85 \cdot 10^{-3} \text{ mol s}^{-1}$  corresponding to 350 L STP sam-  
325 pled in 1200 s, inlet/tubing volume gauged to yield exposure times of 0.01 to 0.1 s due to varia-  
326 ble air intake rate, [O<sub>3</sub>] of 600 nmol/mol), the overall reaction rate coefficient ( $k_c$  in Eq. (A3)  
327 from Appendix A) must be on the order of  $(6 \cdot 10^{-15} / \tau_c) \text{ molecules}^{-1} \text{ cm}^3$ , where  $\tau_c$  is the exposure  
328 time. Assuming the case of a gas-phase CO production from a recombining O<sub>3</sub> derivative and  
329 an unknown carbonaceous compound X, the reaction rate coefficient for the latter ( $k$  in Eq. (A2)  
330 in Appendix A) must be unrealistically high, at least  $6 \cdot 10^{-10} \text{ molec}^{-1} \text{ cm}^3 \text{ s}^{-1}$  over  $\tau_c = 1/100 \text{ s}$ .

331 This number decreases proportionally with growing  $\tau_c$  and  $[X]$ , if we take less strict exposure  
332 conditions. Nonetheless, in order to provide the amounts of artefact CO we detect, a minimum  
333 mixing ratio of 20 nmol/mol (or up to 4  $\mu\text{g}$  of C per flight) of X is required, which is not availa-  
334 ble in the UT/LMS from the species readily undergoing ozonolysis, *e.g.* alkenes.

335 [23] Second, a more complex heterogeneous chemistry on the inner surface of the inlet or sup-  
336 plying tubing may be involved. Such can be the tracers' surface adsorption, (catalytic) decom-  
337 position of  $\text{O}_3$  and its reaction with organics or with surface carbon that also may lead to the  
338 production of CO (Oyama, 2000). Evidence exists for the dissociative adsorption of  $\text{O}_3$  on the  
339 surfaces with subsequent production of the reactive atomic oxygen species (see, *e.g.*,  
340 Li *et al.*, 1998, also Oyama, 2000). It is probable that sufficient amounts of organics have re-  
341 mained on the walls of the sampling line exposed to highly polluted tropospheric air, to be later  
342 broken down by the products of the heterogeneous decomposition of the ample stratospheric  $\text{O}_3$ .  
343 Unfortunately, the scope for a detailed quantification of intricate surface effects in the C1 CO  
344 contamination problem is very limited.

## 345 4 Conclusions

346 [24] Recapitulating, the *in situ* measurements of CO and  $\text{O}_3$  allowed us to unambiguously quanti-  
347 fy the artefact CO production from  $\text{O}_3$  likely in the sample line of the CARIBIC-1 instrumenta-  
348 tion. Strong evidence to that is provided by the isotope CO measurements. We demonstrate the  
349 ability of the simple mixing model ("Keeling-plot" approach) to single out the contamination  
350 isotope signatures even in the case of a large sampling-induced mixing of the air with very dif-  
351 ferent compositions. Obtained as a collateral result, the estimate of the  $\delta^{18}\text{O}(\text{O}_3)$  in the UT/LMS  
352 appears adequate, calling, however, for additional laboratory data (*e.g.*, the temperature-driven  
353 variations of the  $\text{O}_3$  formation KIE at pressures above 100 hPa) for a more unambiguous verifi-  
354 cation.

## 355 Appendix A. Contamination assessment

356 [25] We quantify the C1 CO contamination strength (denoted  $[\text{CO}]_c$ , obtained by discriminating  
357 the C1 outliers from respective C2 data) in a sequence of regression analyses. We foremost as-  
358 certain that no other species or operational parameter (*e.g.* temperature, pressure, flight dura-  
359 tion, season, latitude, time of day, *etc.*) measured in C1 appear to determine (*e.g.*, systematically  
360 correlate with)  $[\text{CO}]_c$ , except that for  $[\text{O}_3]$ . We hypothesise therefore that a production of arte-

361 fact CO molecules was initiated by O<sub>3</sub> (via either its decomposition or a reaction with an un-  
 362 known educt) and proceeded with incorporation of carbon (donated by some carbonaceous spe-  
 363 cies X) and oxygen (donated by O<sub>3</sub> or its derivatives) atoms into final CO. Despite that neither  
 364 the actual reaction chain nor its intermediates are known, it is possible to describe the artefact  
 365 CO component produced (hereinafter curly brackets {} denote number densities) as

$$\{\text{CO}\}_c = \lambda_{\text{O}_3} \nu \tau_c, \quad (\text{A1})$$

366 where the yield  $\lambda_{\text{O}_3}$ , a diagnostic quantity, relates the amount of artefact CO molecules produced  
 367 to the total number of O<sub>3</sub> molecules consumed in the system,  $\tau_c$  denotes the reaction time (peri-  
 368 od throughout which sampled air is exposed to contamination), and  $\nu$  stands for the overall rate  
 369 of the reaction chain. The latter, being regarded macroscopically (empirically), is parameterised  
 370 to account for the order of reaction chain rate with respect to hypothesised reactants  
 371 (McNaught and Wilkinson, 1997) as

$$\nu = k \{\text{X}\}^K \{\text{O}_3\}^\kappa, \quad (\text{A2})$$

372 where  $\kappa$  and  $K$  are the partial orders with respect to X and O<sub>3</sub> number densities, respectively,  
 373 and  $k$  is the rate coefficient. Here it is implied that changes to  $\{\text{X}\}$  and  $\{\text{O}_3\}$  are negligible  
 374 throughout the exposure time  $\tau_c$  (typically < 0.1 s for C1 sample line). As stated above, we find  
 375 that variations in  $\{\text{CO}\}_c$  correlate exclusively with variations in  $\{\text{O}_3\}$ , hence Eq. (A2) can be  
 376 reduced by assuming constancy of  $\{\text{X}\}$  and  $K$  to:

$$\nu_c = k_c \{\text{O}_3\}^\kappa. \quad (\text{A3})$$

377 Here,  $k_c = k \{\text{X}\}^K$  (often referred to as pseudo-first-order or “observed” rate coefficient) quanti-  
 378 fies the rate of reaction chain exclusively propelled by O<sub>3</sub>. Finally, using Eqs. (A1) and (A3),  
 379 the artefact  $\{\text{CO}\}_c$  component is expressed as

$$\{\text{CO}\}_c = b \cdot \{\text{O}_3\}^\kappa, \quad b = \lambda_{\text{O}_3} k_c \tau_c \quad (\text{A4})$$

380 where the constant proportionality factor  $b$  integrates the influence of the unknown (and as we  
 381 explicate below, likely invariable)  $\{\text{X}\}$ ,  $k$ ,  $K$  and  $\tau_c$ .

382 [26] Eq. (A4) defines the regression expression using which we attempt to fit the values of  
 383  $\{\text{CO}\}_c$  as a function of  $\kappa$ ,  $\{\text{O}_3\}$  and  $b$ . In the first regression iteration we keep both  $\kappa$  and  $b$   
 384 as free parameters, which provides best approximation at  $\kappa = 2.06 \pm 0.38$ , suggesting reactions of  
 385 two O<sub>3</sub> molecules in case elementary reactions constitute the reaction mechanism, or two ele-  
 386 mentary steps involving O<sub>3</sub> or its derivatives in case a stepwise reaction is involved  
 387 (McNaught and Wilkinson, 1997). In a subsequent regression iteration we set  $\kappa = 2$ , which  
 388 yields better (as opposed to the first iteration) estimate of  $b$  of  $(5.19 \pm 0.12) \cdot 10^{-5}$  mol/nmol ( $\pm 1\sigma$ ,

389 adj.  $R^2 = 0.83$ , red.  $\chi^2 = 4.0$ ; here the equivalent value in mole fraction units is quoted for the  
390 convenience of relating fitted  $[\text{CO}]_c$  and  $[\text{O}_3]^2$ ). At last, we ascertain that the best regression re-  
391 sults are obtained particularly at  $\kappa = 2$ , as indicated by the regression statistic ( $R^2$  and  $\chi^2$ ) that  
392 asymptotically improves when a set of regressions with neighbouring (*i.e.* below and above 2)  
393 integer values of  $\kappa$  is compared. The low uncertainty (within  $\pm 3\%$ ) associated with the estimate  
394 of  $b$  confirms an exclusive dependence of the contamination source on the  $\text{O}_3$  mixing ratio, as  
395 well as much similar reaction times  $\tau_c$ . The regressed value of  $[\text{CO}]_c$  as a function of  $[\text{O}_3]$  is pre-  
396 sented in Fig. 1 (d) (solid line). It is possible to constrain the overall yield  $\lambda_{\text{O}_3}$  of CO molecules  
397 in the artefact source chain to be between 0.5 and 1, comparing the magnitude of  $[\text{CO}]_c$  to the  
398 discrepancy between the  $[\text{O}_3]$  measured in C1 and C2 ( $\pm 20$  nmol/mol, taken equal to the  $[\text{O}_3]$   
399 bin size owing to the  $\text{N}_2\text{O}-\text{O}_3$  and  $\text{H}_2\text{O}-\text{O}_3$  distributions matching well between the datasets).  
400 Lower  $\lambda_{\text{O}_3}$  values, otherwise, should have resulted in a noticeable (*i.e.*, greater than  
401 20 nmol/mol) decrease in the C1  $\text{O}_3$  mixing ratios with respect to the C2 levels.

## 402 **Appendix B. Corrections to measured $\delta^{13}\text{C}(\text{CO})$ values due to the oxygen**

### 403 **MIF**

404 [27] Atmospheric  $\text{O}_3$  carries an anomalous isotope composition (or mass-independent fractiona-  
405 tion, MIF) with a substantially higher relative enrichment in  $^{17}\text{O}$  over that in  $^{18}\text{O}$  (above  $+25\%$   
406 in  $\Delta^{17}\text{O} = (\delta^{17}\text{O}+1)/(\delta^{18}\text{O}+1)^\beta - 1$ ,  $\beta = 0.528$ ) when compared to the majority of terrestrial oxy-  
407 gen reservoirs that are mass-dependently fractionated (*i.e.*, with  $\Delta^{17}\text{O}$  of  $0\%$ ) (see Brenninkmeij-  
408 er *et al.* (2003) and refs. therein). CO itself also has an unusual oxygen isotopic composition,  
409 possessing a moderate tropospheric MIF of around  $+5\%$  in  $\Delta^{17}\text{O}(\text{CO})$  induced by the sink KIEs  
410 in reaction of CO with OH (Röckmann *et al.*, 1998b; Röckmann *et al.*, 2002) and a minor  
411 source effect from the ozonolysis of alkenes (Röckmann *et al.*, 1998a; Gromov *et al.*, 2010). A  
412 substantial contamination of CO by  $\text{O}_3$  oxygen induces proportional changes to  $\Delta^{17}\text{O}(\text{CO})$  that  
413 largely exceed its natural atmospheric variation. On the other hand, the MIF has implications in  
414 the analytical determination of  $\delta^{13}\text{C}(\text{CO})$ , because the presence of  $\text{C}^{17}\text{O}$  species interferes with  
415 the mass-spectrometric measurement of the abundances of  $^{13}\text{CO}$  possessing the same basic mo-  
416 lecular mass ( $m/z$  is 45). When inferring the exact  $\text{C}^{17}\text{O}/\text{C}^{18}\text{O}$  ratio in the analysed sample is not  
417 possible, analytical techniques usually involve assumptions (*e.g.*, mass-dependently fractionated  
418 compositions or a certain non-zero  $\Delta^{17}\text{O}$  value) with respect to the  $\text{C}^{17}\text{O}$  abundances  
419 (Assonov and Brenninkmeijer, 2001). In effect for the C1 CO data, the artefact CO produced

420 from O<sub>3</sub> had contributed with unexpectedly high C<sup>17</sup>O abundances that led to the overestimated  
421 δ<sup>13</sup>C(CO) analysed. The respective bias <sup>13</sup>δ<sub>b</sub> is quantified using

$$^{13}\delta_b = 7.26 \cdot 10^{-2} \Delta^{17}\text{O}(\text{CO}), \quad (\text{B1})$$

422 where the actual Δ<sup>17</sup>O(CO) value is approximated from the natural CO MIF signal <sup>17</sup>Δ<sub>n</sub> and the  
423 typical O<sub>3</sub> MIF composition <sup>17</sup>Δ<sub>c</sub> as

$$\Delta^{17}\text{O}(\text{CO}) = ({}^{17}\Delta_n ([\text{CO}]_a - [\text{CO}]_c) + {}^{17}\Delta_c [\text{CO}]_c) ([\text{CO}]_a)^{-1}. \quad (\text{B2})$$

424 Here [CO]<sub>a</sub> and [CO]<sub>c</sub> denote the analysed CO mixing ratio and contamination magnitude, re-  
425 spectively, used in the contamination assessment (see Appendix A, Eq. (A3)) and in calcula-  
426 tions with the MM (see Sect. 3.1). For the purpose of the current estimate it is sufficient to take  
427 <sup>17</sup>Δ<sub>n</sub> of +5‰ representing equilibrium enrichments expected in the remote free troposphere and  
428 UT/LMS. For the O<sub>3</sub> MIF signature <sup>17</sup>Δ<sub>c</sub>, the value of +30‰ (the average Δ<sup>17</sup>O(O<sub>3</sub>) expected  
429 from the kinetic laboratory data at conditions met along the C1 flight routes, see Sect. 3.2 and  
430 Table 1) is adopted. The coefficient that proportionates <sup>13</sup>δ<sub>b</sub> and Δ<sup>17</sup>O in Eq. (B1) is derived by  
431 linearly regressing the δ<sup>13</sup>C(CO) biases (simulated using the calculation apparatus detailed by  
432 Assonov and Brenninkmeijer, 2001) as a function of Δ<sup>17</sup>O(CO) varying within a (0–30)‰  
433 range for the CO with initially unaccounted MIF (*e.g.*, the sample is assumed to be mass-  
434 dependently fractionated). It therefore quantifies some extra +(0.726±0.003)‰ in the analysed  
435 δ<sup>13</sup>C(CO) per every +10‰ of Δ<sup>17</sup>O(CO) excess. The most contaminated C1 WAS CO samples  
436 at [O<sub>3</sub>] above 300 nmol/mol are estimated to bear Δ<sup>17</sup>O(CO) of (6–12)‰ corresponding to frac-  
437 tions of (0.10–0.27) of the artefact CO in the sample. Accordingly, the reckoned δ<sup>13</sup>C(CO) bi-  
438 ases span (0.5–0.9)‰. Although not large, these well exceed the δ<sup>13</sup>C(CO) measurement preci-  
439 sion of ±0.1‰ and were corrected for, and therefore are taken into account in the calculations  
440 with the MM presented in Sect. 3.1.

## 441 **Acknowledgements**

442 [28] The authors are indebted to Claus Koepfel, Dieter Scharffe and Dr. Andreas Zahn for their  
443 work and expertise on the carbon monoxide and ozone measurements in C1 and C2. Hella  
444 Riede is acknowledged for comprehensive estimates of the species lifetimes along the  
445 CARIBIC flight routes. We are grateful to Dr. Taku Umezawa, Dr. Angela K. Baker, Dr. Em-  
446 ma C. Leedham, Dr. Sergey Assonov, the anonymous reviewer and Dr. Jan Kaiser for the help-  
447 ful discussions and comments on the manuscript.

## References

- 449 Assonov, S. S. and Brenninkmeijer, C. A. M.: A new method to determine the  $^{17}\text{O}$  isotopic abundance in  
 450  $\text{CO}_2$  using oxygen isotope exchange with a solid oxide, *Rapid Commun. Mass Spectrom.*, **15**,  
 451 2426–2437, doi: [10.1002/rcm.529](https://doi.org/10.1002/rcm.529), 2001.
- 452 Assonov, S. S. and Brenninkmeijer, C. A. M.: A redetermination of absolute values for  $^{17}\text{R}_{\text{VPDB-CO}_2}$  and  
 453  $^{17}\text{R}_{\text{VSMOW}}$ , *Rapid Commun. Mass Spectrom.*, **17**, 1017–1029, doi: [10.1002/Rcm.1011](https://doi.org/10.1002/Rcm.1011), 2003.
- 454 Assonov, S. S., Brenninkmeijer, C. A. M., Koeppel, C., and Röckmann, T.:  $\text{CO}_2$  isotope analyses using  
 455 large air samples collected on intercontinental flights by the CARIBIC Boeing 767,  
 456 *Rapid Commun. Mass Spectrom.*, **23**, 822–830, doi: [10.1002/rcm.3946](https://doi.org/10.1002/rcm.3946), 2009.
- 457 Bhattacharya, S. K., Pandey, A., and Savarino, J.: Determination of intramolecular isotope distribution of  
 458 ozone by oxidation reaction with silver metal, *J. Geophys. Res. Atm.*, **113**, D033303,  
 459 doi: [10.1029/2006jd008309](https://doi.org/10.1029/2006jd008309), 2008.
- 460 Brenninkmeijer, C. A. M.: Measurement of the abundance of  $^{14}\text{CO}$  in the atmosphere and the  $^{13}\text{C}/^{12}\text{C}$  and  
 461  $^{18}\text{O}/^{16}\text{O}$  ratio of atmospheric CO with applications in New Zealand and  
 462 Antarctica, *J. Geophys. Res. Atm.*, **98**, 10595–10614, doi: [10.1029/93JD00587](https://doi.org/10.1029/93JD00587), 1993.
- 463 Brenninkmeijer, C. A. M., Müller, R., Crutzen, P. J., Lowe, D. C., Manning, M. R., Sparks, R. J., and van  
 464 Velthoven, P. F. J.: A large  $^{13}\text{CO}$  deficit in the lower Antarctic stratosphere due to “Ozone Hole”  
 465 Chemistry: Part I, Observations, *Geophys. Res. Lett.*, **23**, 2125–2128, doi: [10.1029/96gl01471](https://doi.org/10.1029/96gl01471), 1996.
- 466 Brenninkmeijer, C. A. M. and Röckmann, T.: Principal factors determining the  $^{18}\text{O}/^{16}\text{O}$  ratio of  
 467 atmospheric CO as derived from observations in the southern hemispheric troposphere and lowermost  
 468 stratosphere, *J. Geophys. Res. Atm.*, **102**, 25477–25485, doi: [10.1029/97JD02291](https://doi.org/10.1029/97JD02291), 1997.
- 469 Brenninkmeijer, C. A. M., Crutzen, P. J., Fischer, H., Gusten, H., Hans, W., Heinrich, G.,  
 470 Heintzenberg, J., Hermann, M., Immelmann, T., Kersting, D., Maiss, M., Nolle, M., Pitscheider, A.,  
 471 Pohlkamp, H., Scharffe, D., Specht, K., and Wiedensohler, A.: CARIBIC – Civil aircraft for global  
 472 measurement of trace gases and aerosols in the tropopause region, *J. Atmos. Oceanic Technol.*, **16**,  
 473 1373–1383, doi: [10.1175/1520-0426\(1999\)016<1373:Ccafgm>2.0.Co;2](https://doi.org/10.1175/1520-0426(1999)016<1373:Ccafgm>2.0.Co;2), 1999.
- 474 Brenninkmeijer, C. A. M., Koeppel, C., Röckmann, T., Scharffe, D. S., Bränlich, M., and Gros, V.:  
 475 Absolute measurement of the abundance of atmospheric carbon monoxide, *J. Geophys. Res. Atm.*, **106**,  
 476 10003–10010, doi: [10.1029/2000jd900342](https://doi.org/10.1029/2000jd900342), 2001.
- 477 Brenninkmeijer, C. A. M., Janssen, C., Kaiser, J., Röckmann, T., Rhee, T. S., and Assonov, S. S.: Isotope  
 478 effects in the chemistry of atmospheric trace compounds, *Chem. Rev.*, **103**, 5125–5161,  
 479 doi: [10.1021/Cr020644k](https://doi.org/10.1021/Cr020644k), 2003.
- 480 Brenninkmeijer, C. A. M., Crutzen, P., Boumard, F., Dauer, T., Dix, B., Ebinghaus, R., Filippi, D.,  
 481 Fischer, H., Franke, H., Frieß, U., Heintzenberg, J., Helleis, F., Hermann, M., Kock, H. H.,  
 482 Koeppel, C., Lelieveld, J., Leuenberger, M., Martinsson, B. G., Miemczyk, S., Moret, H. P.,  
 483 Nguyen, H. N., Nyfeler, P., Oram, D., O'Sullivan, D., Penkett, S., Platt, U., Pupek, M., Ramonet, M.,  
 484 Randa, B., Reichelt, M., Rhee, T. S., Rohwer, J., Rosenfeld, K., Scharffe, D., Schlager, H.,  
 485 Schumann, U., Slemr, F., Sprung, D., Stock, P., Thaler, R., Valentino, F., van Velthoven, P.,  
 486 Waibel, A., Wandel, A., Waschitschek, K., Wiedensohler, A., Xueref-Remy, I., Zahn, A.,  
 487 Zech, U., and Ziereis, H.: Civil Aircraft for the regular investigation of the atmosphere based on an  
 488 instrumented container: The new CARIBIC system, *Atmos. Chem. Phys.*, **7**, 4953–4976,  
 489 doi: [10.5194/acp-7-4953-2007](https://doi.org/10.5194/acp-7-4953-2007), 2007.



490 Coplen, T. B.: Reporting of stable hydrogen, carbon, and oxygen isotopic abundances (Technical Report),  
491 *Pure Appl. Chem.*, **66**, 273–276, doi: [10.1351/pac199466020273](https://doi.org/10.1351/pac199466020273), 1994.

492 Craig, H.: Isotopic standards for carbon and oxygen and correction factors for mass-spectrometric analysis  
493 of carbon dioxide, *Geochim. Cosmochim. Acta*, **12**, 133–149, doi: [10.1016/0016-7037\(57\)90024-8](https://doi.org/10.1016/0016-7037(57)90024-8),  
494 1957.

495 Gonfiantini, R.: Standards for Stable Isotope Measurements in Natural Compounds, *Nature*, **271**,  
496 534–536, 1978.

497 Gromov, S., Jöckel, P., Sander, R., and Brenninkmeijer, C. A. M.: A kinetic chemistry tagging technique  
498 and its application to modelling the stable isotopic composition of atmospheric trace gases,  
499 *Geosci. Model Dev.*, **3**, 337–364, doi: [10.5194/gmd-3-337-2010](https://doi.org/10.5194/gmd-3-337-2010), 2010.

500 Guenther, J., Erbacher, B., Krankowsky, D., and Mauersberger, K.: Pressure dependence of two relative  
501 ozone formation rate coefficients, *Chem. Phys. Lett.*, **306**, 209–213,  
502 doi: [10.1016/S0009-2614\(99\)00469-8](https://doi.org/10.1016/S0009-2614(99)00469-8), 1999.

503 Janssen, C., Guenther, J., Krankowsky, D., and Mauersberger, K.: Temperature dependence of ozone rate  
504 coefficients and isotopologue fractionation in  $^{16}\text{O}$ – $^{18}\text{O}$  oxygen mixtures, *Chem. Phys. Lett.*, **367**,  
505 34–38, doi: [10.1016/S0009-2614\(02\)01665-2](https://doi.org/10.1016/S0009-2614(02)01665-2), 2003.

506 Janssen, C.: Intramolecular isotope distribution in heavy ozone ( $^{16}\text{O}^{18}\text{O}^{16}\text{O}$  and  $^{16}\text{O}^{16}\text{O}^{18}\text{O}$ ),  
507 *J. Geophys. Res. Atm.*, **110**, D08308, doi: [10.1029/2004jd005479](https://doi.org/10.1029/2004jd005479), 2005.

508 Johnston, J. C. and Thiemens, M. H.: The isotopic composition of tropospheric ozone in three  
509 environments, *J. Geophys. Res. Atm.*, **102**, 25395–25404, doi: [10.1029/97jd02075](https://doi.org/10.1029/97jd02075), 1997.

510 Krankowsky, D., Bartecki, F., Klees, G. G., Mauersberger, K., Schellenbach, K., and Stehr, J.:  
511 Measurement of heavy isotope enrichment in tropospheric ozone, *Geophys. Res. Lett.*, **22**, 1713–1716,  
512 doi: [10.1029/95gl01436](https://doi.org/10.1029/95gl01436), 1995.

513 Krankowsky, D., Lämmerzahl, P., Mauersberger, K., Janssen, C., Tuzson, B., and Röckmann, T.:  
514 Stratospheric ozone isotope fractionations derived from collected samples, *J. Geophys. Res. Atm.*, **112**,  
515 D08301, doi: [10.1029/2006jd007855](https://doi.org/10.1029/2006jd007855), 2007.

516 Li, W., Gibbs, G. V., and Oyama, S. T.: Mechanism of Ozone Decomposition on a Manganese Oxide  
517 Catalyst. 1. In Situ Raman Spectroscopy and Ab Initio Molecular Orbital  
518 Calculations, *J. Am. Chem. Soc.*, **120**, 9041–9046, doi: [10.1021/ja981441+](https://doi.org/10.1021/ja981441+), 1998.

519 Mauersberger, K.: Measurement of Heavy Ozone in the Stratosphere, *Geophys. Res. Lett.*, **8**, 935–937,  
520 doi: [10.1029/G1008i008p00935](https://doi.org/10.1029/G1008i008p00935), 1981.

521 McNaught, A. D. and Wilkinson, A.: IUPAC. Compendium of Chemical Terminology (the "Gold Book"),  
522 XML on-line corrected version: <http://goldbook.iupac.org> (2006-) created by  
523 M. Nic, J. Jirat, B. Kosata; updates compiled by A. Jenkins, doi: [10.1351/goldbook.O04322](https://doi.org/10.1351/goldbook.O04322), 1997.

524 Natrella, M.: NIST/SEMATECH e-Handbook of Statistical Methodsed., edited by: Croarkin, C. and  
525 Tobias, P., NIST/SEMATECH, <http://www.itl.nist.gov/div898/handbook/> (last access: 07 May 2014),  
526 2003.

527 Novelli, P. C., Masarie, K. A., and Lang, P. M.: Distributions and recent changes of carbon monoxide in  
528 the lower troposphere, *J. Geophys. Res.*, **103**, 19015–19033, doi: [10.1029/98jd01366](https://doi.org/10.1029/98jd01366), 1998.

529 Novelli, P. C., Masarie, K. A., Lang, P. M., Hall, B. D., Myers, R. C., and Elkins, J. W.: Reanalysis of  
530 tropospheric CO trends: Effects of the 1997–1998 wildfires, *J. Geophys. Res.*, **108**, 4464,  
531 doi: [10.1029/2002jd003031](https://doi.org/10.1029/2002jd003031), 2003.

- 532 Oyama, S. T.: Chemical and Catalytic Properties of Ozone, *Catal. Rev. Sci. Eng.*, **42**, 279–322,  
533 doi: [10.1081/cr-100100263](https://doi.org/10.1081/cr-100100263), 2000.
- 534 Pan, L. L., Randel, W. J., Gary, B. L., Mahoney, M. J., and Hints, E. J.: Definitions and sharpness of the  
535 extratropical tropopause: A trace gas perspective, *J. Geophys. Res. Atm.*, **109**, D23103,  
536 doi: [10.1029/2004jd004982](https://doi.org/10.1029/2004jd004982), 2004.
- 537 Röckmann, T., Brenninkmeijer, C. A. M., Neeb, P., and Crutzen, P. J.: Ozonolysis of nonmethane  
538 hydrocarbons as a source of the observed mass independent oxygen isotope enrichment in tropospheric  
539 CO, *J. Geophys. Res. Atm.*, **103**, 1463–1470, doi: [10.1029/97JD02929](https://doi.org/10.1029/97JD02929), 1998a.
- 540 Röckmann, T., Brenninkmeijer, C. A. M., Saueressig, G., Bergamaschi, P., Crowley, J. N.,  
541 Fischer, H., and Crutzen, P. J.: Mass-independent oxygen isotope fractionation in atmospheric CO as a  
542 result of the reaction CO+OH, *Science*, **281**, 544–546, doi: [10.1126/science.281.5376.544](https://doi.org/10.1126/science.281.5376.544), 1998b.
- 543 Röckmann, T., Jöckel, P., Gros, V., Bräunlich, M., Possnert, G., and Brenninkmeijer, C. A. M.: Using <sup>14</sup>C,  
544 <sup>13</sup>C, <sup>18</sup>O and <sup>17</sup>O isotopic variations to provide insights into the high northern latitude surface CO  
545 inventory, *Atmos. Chem. Phys.*, **2**, 147–159, doi: [10.5194/acp-2-147-2002](https://doi.org/10.5194/acp-2-147-2002), 2002.
- 546 Savarino, J., Bhattacharya, S. K., Morin, S., Baroni, M., and Doussin, J. F.: The NO+O<sub>3</sub> reaction: A triple  
547 oxygen isotope perspective on the reaction dynamics and atmospheric implications for the transfer of  
548 the ozone isotope anomaly, *J. Chem. Phys.*, **128**, 194303, doi: [10.1063/1.2917581](https://doi.org/10.1063/1.2917581), 2008.
- 549 Savarino, J. and Morin, S.: The N, O, S Isotopes of Oxy-Anions in Ice Cores and Polar Environments, in:  
550 Handbook of Environmental Isotope Geochemistry, edited by: Baskaran, M., Advances in Isotope  
551 Geochemistry, Springer Berlin Heidelberg, 835–864, 2012.
- 552 Scharffe, D., Slemr, F., Brenninkmeijer, C. A. M., and Zahn, A.: Carbon monoxide measurements onboard  
553 the CARIBIC passenger aircraft using UV resonance fluorescence, *Atmos. Meas. Tech.*, **5**, 1753–1760,  
554 doi: [10.5194/amt-5-1753-2012](https://doi.org/10.5194/amt-5-1753-2012), 2012.
- 555 Schinke, R., Grebenshchikov, S. Y., Ivanov, M. V., and Fleurat-Lessard, P.: Dynamical Studies Of The  
556 Ozone Isotope Effect: A Status Report, *Annu. Rev. Phys. Chem.*, **57**, 625–661,  
557 doi: [10.1146/annurev.physchem.57.032905.104542](https://doi.org/10.1146/annurev.physchem.57.032905.104542), 2006.
- 558 Stevens, C. M., Kaplan, L., Gorse, R., Durkee, S., Compton, M., Cohen, S., and Bielling, K.: The Kinetic  
559 Isotope Effect for Carbon and Oxygen in the Reaction CO+OH, *Int. J. Chem. Kinet.*, **12**, 935–948,  
560 doi: [10.1002/kin.550121205](https://doi.org/10.1002/kin.550121205), 1980.
- 561 Vicars, W. C., Bhattacharya, S. K., Erbland, J., and Savarino, J.: Measurement of the <sup>17</sup>O-excess ( $\Delta^{17}\text{O}$ ) of  
562 tropospheric ozone using a nitrite-coated filter, *Rapid Commun. Mass Spectrom.*, **26**, 1219–1231,  
563 doi: [10.1002/rcm.6218](https://doi.org/10.1002/rcm.6218), 2012.
- 564 Vicars, W. C. and Savarino, J.: Quantitative constraints on the <sup>17</sup>O-excess ( $\Delta^{17}\text{O}$ ) signature of surface  
565 ozone: Ambient measurements from 50°N to 50°S using the nitrite-coated filter technique,  
566 *Geochim. Cosmochim. Acta*, **135**, 270–287, doi: [10.1016/j.gca.2014.03.023](https://doi.org/10.1016/j.gca.2014.03.023), 2014.
- 567 Zahn, A., Brenninkmeijer, C. A. M., Maiss, M., Scharffe, D. H., Crutzen, P. J., Hermann, M.,  
568 Heintzenberg, J., Wiedensohler, A., Güsten, H., Heinrich, G., Fischer, H., Cuijpers, J. W. M., and van  
569 Velthoven, P. F. J.: Identification of extratropical two-way troposphere-stratosphere mixing based on  
570 CARIBIC measurements of O<sub>3</sub>, CO, and ultrafine particles, *J. Geophys. Res.*, **105**, 1527–1535,  
571 doi: [10.1029/1999jd900759](https://doi.org/10.1029/1999jd900759), 2000.
- 572 Zahn, A., Brenninkmeijer, C. A. M., Asman, W. A. H., Crutzen, P. J., Heinrich, G., Fischer, H.,  
573 Cuijpers, J. W. M., and van Velthoven, P. F. J.: Budgets of O<sub>3</sub> and CO in the upper troposphere:

574 CARIBIC passenger aircraft results 1997–2001, *J. Geophys. Res. Atm.*, **107**, 4337,  
 575 doi: [10.1029/2001jd001529](https://doi.org/10.1029/2001jd001529), 2002.

576 Zahn, A., Weppner, J., Widmann, H., Schlote-Holubek, K., Burger, B., Kühner, T., and Franke, H.: A fast  
 577 and precise chemiluminescence ozone detector for eddy flux and airborne application,  
 578 *Atmos. Meas. Tech.*, **5**, 363–375, doi: [10.5194/amt-5-363-2012](https://doi.org/10.5194/amt-5-363-2012), 2012.

579

## 580 Tables

581 Table 1. Ozone  $^{18}\text{O}/^{16}\text{O}$  isotope ratios from literature and this study

Domain	T (K)	P (hPa)	$\delta^{18}\text{O}(\text{O}_3)$ (‰)	Remarks
Stratosphere	190–210	13–50	83–93 (<3)	1
UT/LMS	220–235	240–270	89–95 (8)	2
			84–88 (6)	T
			91–98 (9)	TC
			112–124 (17)	C
Laboratory	190–210	67	87–97 (6)	3
	220–235	67	102–110 (6)	3
	220–235	240–270	95–103	4

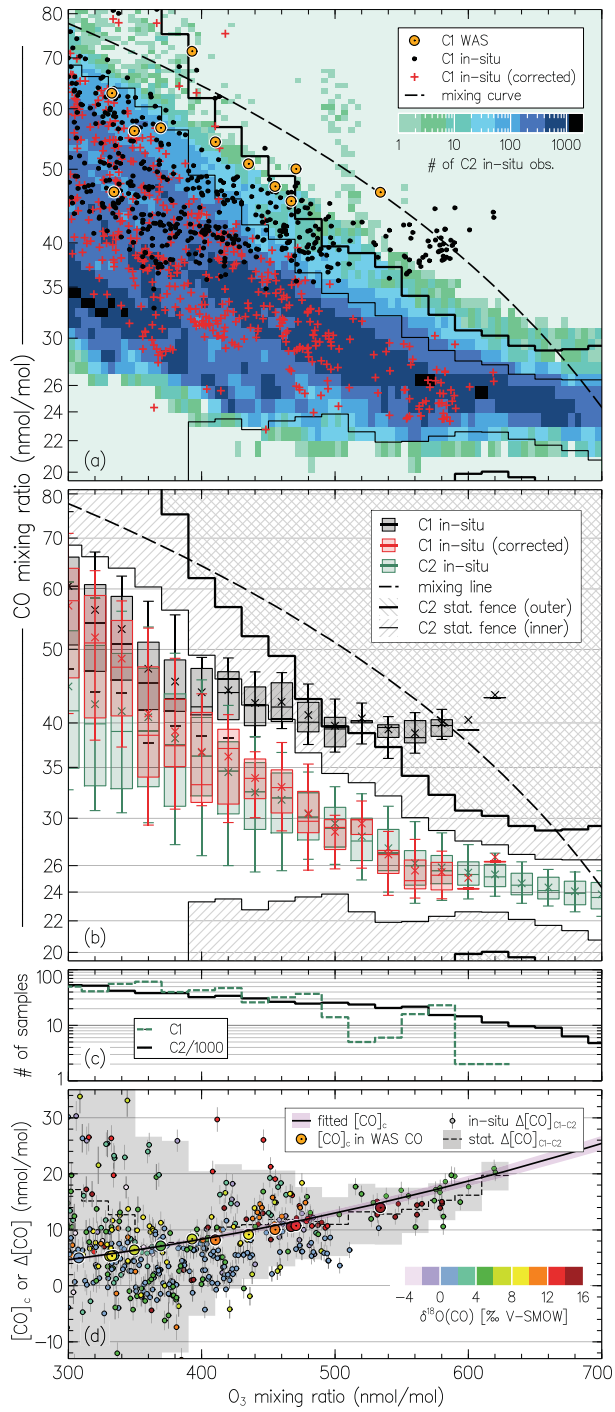
Notes: Values in parentheses denote the average of the estimates' standard errors. The expected  $\text{O}_3$  isotope composition on the VSMOW scale is calculated from the  $\text{O}_3$  enrichments reported relative to  $\text{O}_2$  using  $\delta^{18}\text{O}(\text{O}_3)_{\text{VSMOW}} = \delta^{18}\text{O}(\text{O}_2)_{\text{VSMOW}} + {}^{18}\delta(\text{O}_3)_{\text{Air-O}_2} + [\delta^{18}\text{O}(\text{O}_2)_{\text{VSMOW}} \times {}^{18}\epsilon(\text{O}_3)_{\text{Air-O}_2}]$ .

<sup>1</sup> Observations (see Krankowsky *et al.* (2007) and refs. therein), lowermost values (19–25 km). Quoted temperature range is derived by matching measured  $\delta^{18}\text{O}(\text{O}_3)$  and laboratory data (see note <sup>3</sup>).

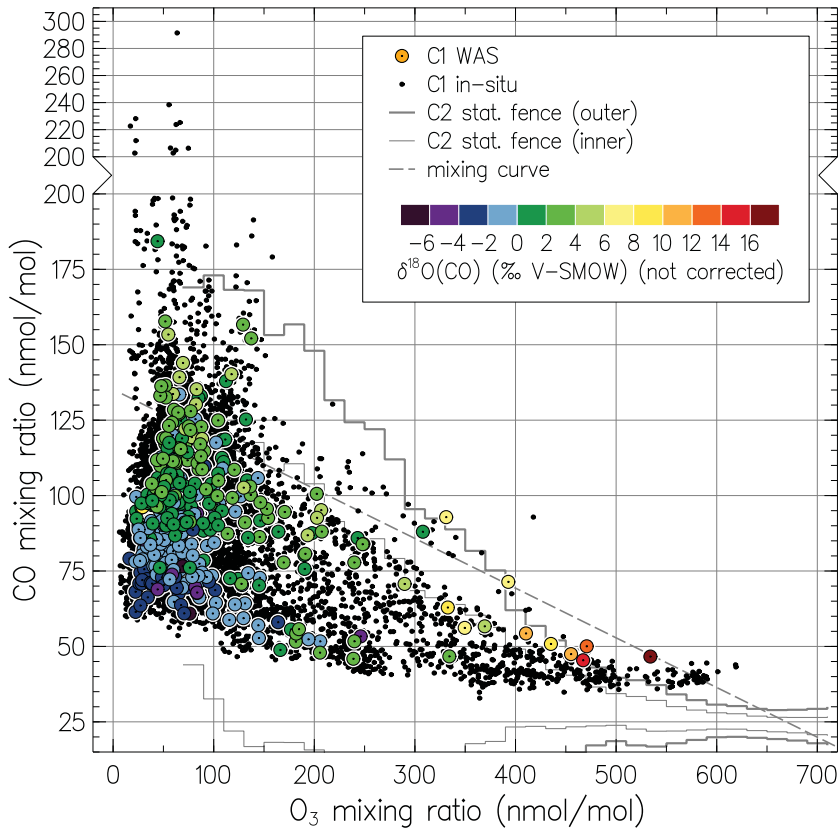
<sup>2</sup> This study, C1 observations (10–12 km). Letters denote the estimates derived using the data from Bhattacharya *et al.* (2008) and assuming only terminal (T), only central (C) and equiprobable terminal and central (TC)  $\text{O}_3$  atoms transfer to the artefact  $\text{CO}$ .

<sup>3</sup> Calculated using the laboratory KIE temperature dependence data summarised by Janssen *et al.* (2003).

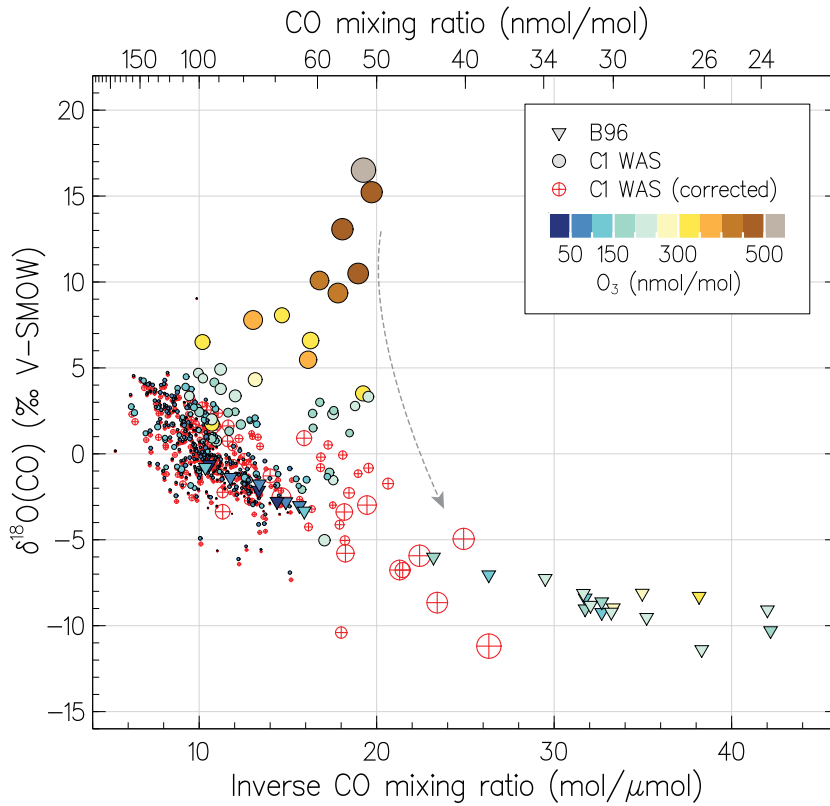
<sup>4</sup> Calculated assuming a pressure dependence of the  $\text{O}_3$  formation KIE similar to that measured at 320 K (see Guenther *et al.* (1999) and refs. therein).



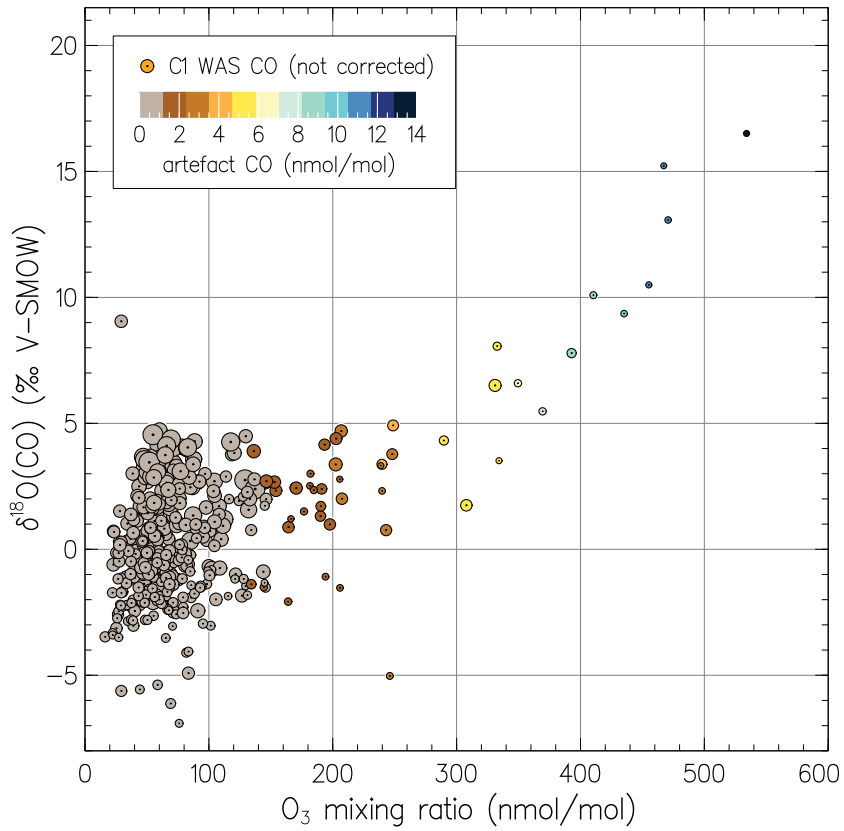
583 Fig. 1. (a) Distribution of CO mixing ratios as a function of concomitant O<sub>3</sub> mixing ratios measured by  
584 CARIBIC in the LMS ([O<sub>3</sub>] > 300 nmol/mol). The shaded area is the two-dimensional histogram of the C2  
585 measurements (all C2 data obtained until June 2013) counted in 5 × 1 nmol/mol size [O<sub>3</sub>] × [CO] bins, thus  
586 darker areas emphasise greater numbers of particular CO–O<sub>3</sub> pairs observed. Small symbols denote the  
587 original C1 *in situ* measurements (black) and corrected for the artefacts (red); the C1 WAS analyses (11 of  
588 total 408) are shown with large symbols. Thin and thick step-lines demark the inner and outer statistical  
589 fences (ranges outside which the data points are considered mild or extreme outliers, see text) of the C2  
590 data, respectively. The dashed curve exemplifies compositions expected from the linear mixing of very  
591 different (*e.g.*, tropospheric and stratospheric) end-members. (b) Statistics on CO mixing ratios from C1  
592 and C2 data shown in box-and-whisker diagrams for samples clustered in 20 nmol/mol O<sub>3</sub> bins (whiskers  
593 represent 9<sup>th</sup>/91<sup>st</sup> percentiles). (c) Sample statistic for each CARIBIC dataset (note the C2 figures scaled  
594 down by a factor of 1000). (d) Estimates of the C1 *in situ* CO contamination strength [CO]<sub>c</sub> as a function  
595 of [O<sub>3</sub>] (solid line) obtained by fitting the difference Δ[CO] between the C2 and C1 *in situ* [CO] (small  
596 symbols) as detailed in Appendix A (Eq. (A1)). Step line shows the Δ[CO] for the statistical averages (the  
597 shaded area equals the height of the inner statistical fences of the C2 data). Large symbols denote the es-  
598 timates of C<sub>c</sub> in the C1 WAS data (slight variations *vs.* the *in situ* data are due to the sample mixing ef-  
599 fects, see Sect. 3). Colour denotes the respective C1 WAS δ<sup>18</sup>O(CO) (note that typically 6–7 *in situ* meas-  
600 urements correspond to one WAS sample).



601 Fig. 2. (accompanies Fig. 1) Carbon monoxide and ozone mixing ratios measured in C1. Small black sym-  
 602 bols denote the C1 *in situ* measurements ( $n = 12753$ ). The C1 WAS analyses ( $n = 408$ ) are shown with  
 603 large symbols; colour denotes the concomitant  $\delta^{18}\text{O}(\text{CO})$  measurements. Thin and thick step-lines denote  
 604 the inner and outer statistical fences of the C2 data, respectively. The dashed curve exemplifies composi-  
 605 tions expected from the linear mixing of tropospheric and stratospheric end-members (see caption to Fig. 1  
 606 for details).

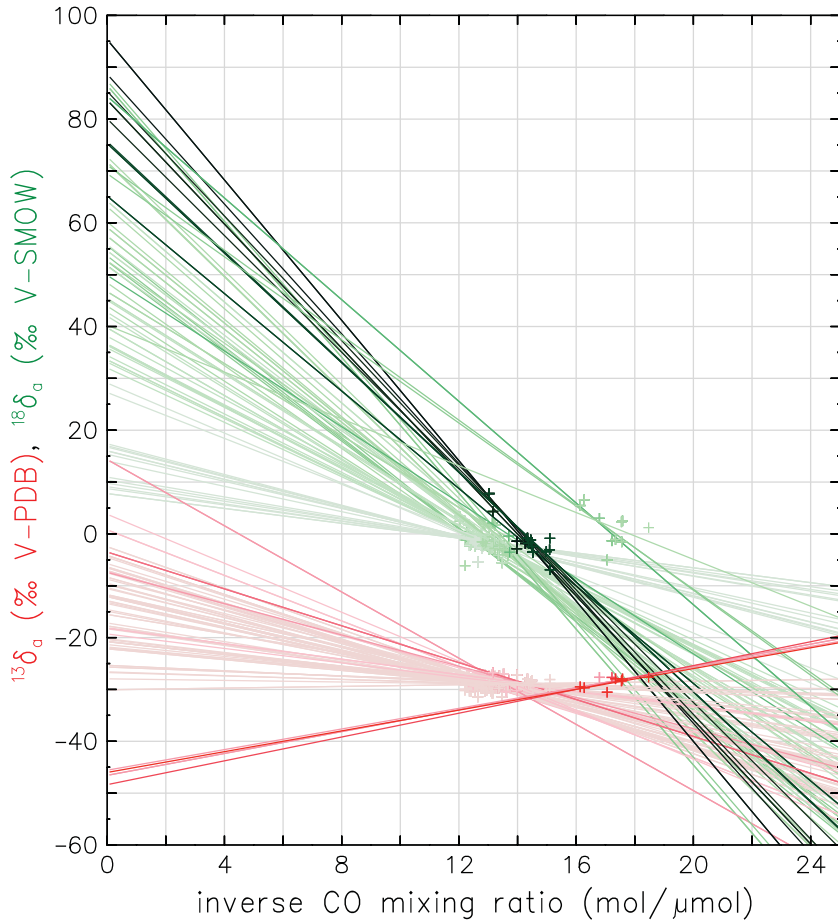


607 Fig. 3.  $^{18}\text{O}/^{16}\text{O}$  isotope composition of CO as a function of its reciprocal mixing ratio. Triangles present  
 608 the data from the remote SH UT/LMS obtained by Brenninkmeijer *et al.* (1996) (B96). Colour refers to the  
 609 concomitantly observed  $\text{O}_3$  abundances; note the extremely low  $[\text{O}_3]$  encountered by B96 in the Antarctic  
 610 "ozone hole" conditions. Filled and hollow circles denote the original and corrected (as exemplified by the  
 611 dashed arrow) C1 WAS data, respectively, with the symbol size scaling proportional to the estimated con-  
 612 tamination magnitude (see text).

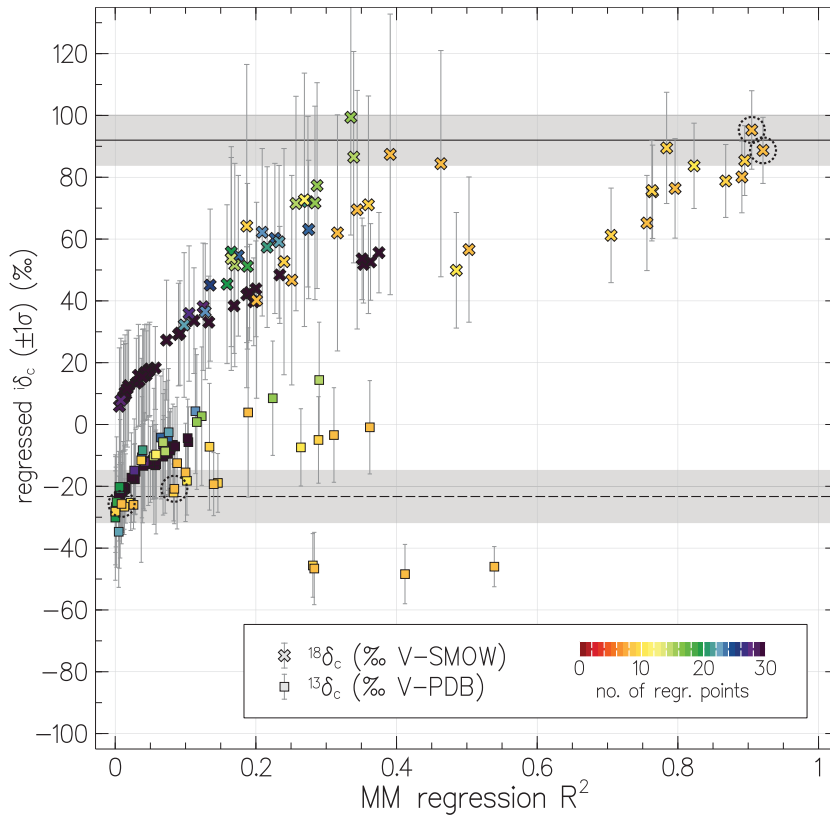


613 Fig. 4. Measured C1 WAS  $\delta^{18}\text{O}(\text{CO})$  (not corrected for artefacts) as a function of concomitant  $\text{O}_3$  mixing  
 614 ratio. Symbol colour denotes the artefact CO component (integral  $[\text{CO}]_c$  per each WAS); symbol size  
 615 scales proportionally to the WAS CO mixing ratio corrected for artefacts (see Sect. 3 for details).

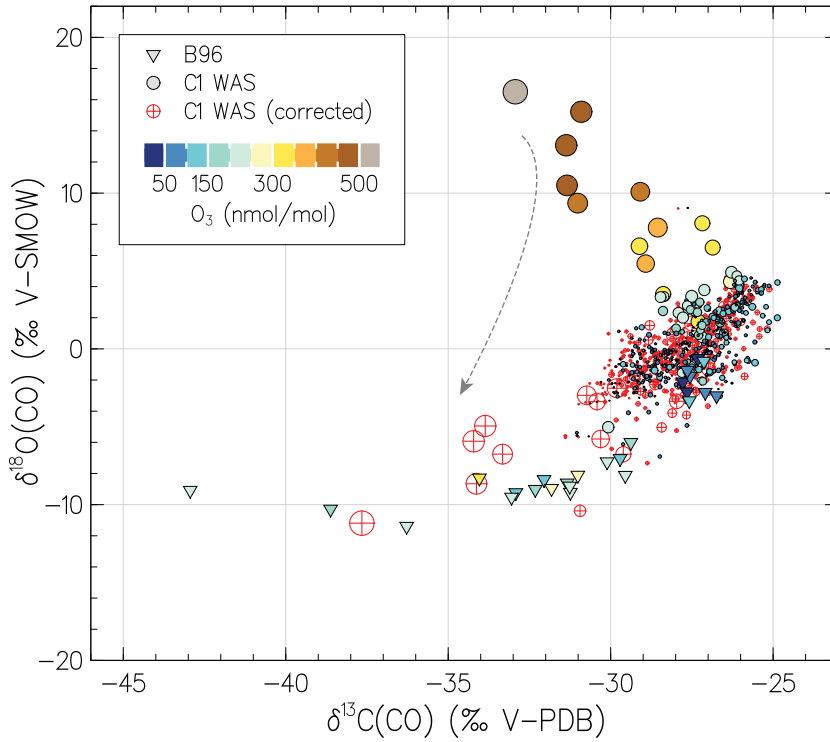




616 Fig. 5. Keeling plot of the data used in the calculations with the mixing model (MM). The C1 WAS iso-  
 617 tope CO measurements are shown with symbols, solid lines denote the linear regressions through the vari-  
 618 ous sets of samples selected by the MM ( $n = 80$  sets are plotted). Colours refer to the  $\delta^{13}\text{C}$  (red) and  $\delta^{18}\text{O}$   
 619 (green) data, colour intensity indicates the coefficient of determination ( $R^2$ ) of each regression, respec-  
 620 tively. Darker colours denote higher  $R^2$  values, with maxima of 0.92 for  $\delta^{18}\text{O}$  and 0.54 for  $\delta^{13}\text{C}$  data, respec-  
 621 tively. The inferred contamination signatures ( $^i\delta_c$ ) are found at  $([\text{CO}]_a)^{-1} \rightarrow 0$ . Regression uncertainties are  
 622 shown in Fig. 6. Note that because different subsets of samples contain same data points, some of the  
 623 symbols are plotted over (*i.e.*, not all symbols contributing to a particular regression case may be seen).



624 Fig. 6. Results of the regression calculation with the MM. Shown with symbols are the contamination  
 625 source isotope signatures  $i\delta_c$  as a function of the respective coefficient of determination ( $R^2$ ). Colour de-  
 626 notes the number of samples in each subset selected. Solid and dashed lines present the best guess  
 627  $\pm 1$  standard deviation of the mean for the  $^{18}\delta_c$  and  $^{13}\delta_c$  estimates. Dashed circles mark the estimates ob-  
 628 tained at highest  $R^2$  for  $^{18}\delta_c$  regression (above 0.9). See text for details.



629 Fig. 7.  $^{18}\text{O}/^{16}\text{O}$  and  $^{13}\text{C}/^{12}\text{C}$  isotope composition of CO measured in C1. Triangles present the data from the  
 630 remote SH UT/LMS obtained by Brenninkmeijer *et al.* (1996) (B96). Colour refers to the concomitantly  
 631 observed  $\text{O}_3$  abundances; note the extremely low  $[\text{O}_3]$  encountered by B96 in the Antarctic ozone-hole  
 632 conditions. Filled and hollow circles denote the original and corrected (as exemplified by the dashed ar-  
 633 row) C1 WAS data, respectively, with the symbol size scaling proportional to the estimated contamination  
 634 magnitude (see text for details).